

# Update of parameter matrices of the dynamic system using the least-squares approach

Advances in Mechanical Engineering  
2019, Vol. 11(11) 1–12  
© The Author(s) 2019  
DOI: 10.1177/1687814019890806  
journals.sagepub.com/home/ade  
 SAGE

Eun-Taik Lee<sup>1</sup> and Hee-Chang Eun<sup>2</sup>

## Abstract

Model-based responses rarely coincide with the actual responses owing to modeling and measurement errors, deterioration of structural performance, and presence of damages in the structure. The parameter matrices should be updated for successful subsequent analysis and design efforts. This study derives the mathematical forms of variations in the parameter matrices between the actual system and the analytical model. A method using the least-squares principle constrained by the measured modal data is presented. The method is directly derived by minimizing the performance indices expressed by the norm of the variation in the parameter matrices between the actual system and the analytical model. The proposed update methods predict the updated parameter matrices depending on the prescribed weighting matrices and detect damages from the predicted parameter matrix variations. Examples compare the methods depending on the established weighting matrices, the number of measurement data sets of the first modal data only and the lowest two modal data. This study also investigates the effect of external noise contained in the measured data.

## Keywords

Damage detection, update of parameter matrices, noise, flexibility matrix, eigenfunction

Date received: 19 April 2019; accepted: 24 October 2019

Handling Editor: Dumitru Baleanu

## Introduction

It is difficult to accurately describe the responses of an actual system using the structural model established at the design stage because of inaccurate constructions, inhomogeneous properties of the structural materials, environmental effects, and measurement errors. The inaccurate utilization of the parameter matrices, such as the mass and stiffness matrices of the dynamic system, leads to the responses being deviated from the initial responses. Such inaccuracies should be minimized for successful subsequent analysis and design.

Numerous studies pertaining to the handling of updated parameter matrices of a finite-element model using only measured data have been reported. The updated parameter matrices can also be utilized as evidence to determine the defect in dynamic systems. The parameter matrices are primarily corrected using the

least-squares methods and the parameter sensitivity methods.

The parameter-updating methods are used for obtaining responses that are as close as possible to the experimental and actual responses. Wang et al.<sup>1</sup> compared the modal parameter-based and flexibility-based damage-identification methods by optimizing the objective functions of a weighted function of the frequency

<sup>1</sup>Department of Architectural Engineering, Chung-Ang University, Seoul, Korea

<sup>2</sup>Department of Architectural Engineering, Kangwon National University, Chuncheon, Korea

## Corresponding author:

Hee-Chang Eun, Department of Architectural Engineering, Kangwon National University, Chuncheon 24341, Korea.  
Email: heechang@kangwon.ac.kr



Creative Commons CC BY: This article is distributed under the terms of the Creative Commons Attribution 4.0 License (<http://www.creativecommons.org/licenses/by/4.0/>) which permits any use, reproduction and distribution of the work

without further permission provided the original work is attributed as specified on the SAGE and Open Access pages (<https://us.sagepub.com/en-us/nam/open-access-at-sage>).

and mode shapes and modal flexibility residue, respectively. Schommer et al.<sup>2</sup> discussed the difference between stiffness and the flexibility matrix for structural health monitoring based on vibrational measurements. They found that the flexibility-based quantification and localization of damage are more difficult. Lekidis et al.<sup>3</sup> developed a finite-element model-updating method based on an incomplete set of modal frequencies and mode shapes. Başıga et al.<sup>4</sup> proposed an updating algorithm for the uncertain parameters for each mode by minimizing the difference between the analytical and experimental natural frequencies. Fuentes<sup>5</sup> introduced and compared analytical methods that combine the mode-shaped expansion methods and the update methods of the stiffness parameters. Rim et al.<sup>6</sup> predicted the updated forms of the parameter matrices based on the estimated mode shape data. Chen and Tee<sup>7</sup> presented the optimized solutions in the least squares from the difference in the structural parameters between the finite-element model and the associated tested structure. Sheinman<sup>8</sup> provided an analytical algorithm for damage detection and for updating parameter matrices using the minimum static and/or dynamic measured modes and preserved the connectivity. Pokharkar and Shrikhande<sup>9</sup> provided an updated time-domain least-squares method to identify the structural stiffness and mass matrices using the condensed model. Sung et al.<sup>10</sup> presented a damage-detection approach for cantilever beam-type structures using the deflection estimated by the modal flexibility matrix. Rainieri et al.<sup>11</sup> provided dynamic identification techniques for the non-destructive evaluation of heritage structures.

Katebi et al.<sup>12</sup> obtained a damage-identification method using changes in the sensitivity matrix and the measured flexibility data. Chen and Nagarajaiah<sup>13</sup> derived the structural parameter optimization method by minimizing the Frobenius norm of the change in the flexibility matrix and the Gauss–Newton method for solving the optimization problem. Li et al.<sup>14</sup> presented a method for detecting reduction in the stiffness parameters of a structure using a generalized flexibility matrix and changes in natural frequencies. Yang and Sun<sup>15</sup> proposed a damage-detection method based on the best achievable flexibility change to localize and quantify damages. Cao et al.<sup>16</sup> proposed a model-updating method based on the residual flexibility mixed-boundary substructure method. Using the linear relationship between the flexibility matrix element and the structural parameter, Yang et al.<sup>17</sup> introduced the modal parameter and damage coefficient and provided a flexibility-based method for identifying the location and extent of the damage. Lacidogna et al.<sup>18</sup> investigated the damage propagation process using the acoustic emission technique and the extraction of resonance frequencies. They also evaluated the damage mechanisms for the stress-dependent damage progress using

the acoustic emission and dynamic identification techniques.<sup>19</sup>

Existing modal identification methods require extensive interaction and computational efforts. There have been research efforts for automated modal identification and tracking procedure. Rainieri and Fabbrocino<sup>20</sup> presented a literature review on automated operational modal analysis and developed algorithm aiming at fully automated output-only modal identification. They also investigated the validity of the automated output-only modal parameter estimation algorithm.<sup>21</sup> Rainieri et al.<sup>22</sup> proposed the use of second-order blind identification to estimate modal property.

The dynamic systems can be modeled by a system of fractional differential equations (FDEs). Using the operational matrix for fractional integral operator based on Chebyshev polynomials, a system of linear algebraic equations is derived and the numerical approximation can be obtained by solving system of Mittag–Leffler non-singular FDEs. Efficient numerical methods to solve a system of Mittag–Leffler non-singular FDEs have been considered.<sup>23–28</sup>

This article presents the mathematical forms of the updated parameter matrices to satisfy the flexibility matrix and eigenfunction established by the measured modal data using the least-squares approach. The update method is straightforwardly derived by minimizing the objective functions to satisfy the measured modal data. The parameter matrices take different mathematical forms depending on the prescribed objective functions and the weighting matrices. The numerical examples exhibit that the stiffness matrix as the weighting matrix indicates more accurate damage information than the mass matrix despite the external noise. It is found that the sensitivity to external noise contained in the measured mode shape data disappears in the use of accumulated data through repeated numerical simulations. The resulting method can be extended for detecting damages using the finite-element method. Furthermore, the predicted parameter matrices compare the validity of the proposed methods depending on the measured number of lowest modal data sets.

The structure of this article is as follows: In section “Estimation of updated stiffness and mass matrices,” we derive the mathematical forms to update stiffness matrix as well as mass matrix, and the corresponding example is presented to illustrate the validity of the proposed methods and to compare the numerical results depending on the presumed weighting matrices. In section “Estimation of updated stiffness matrix,” the mathematical forms to correct stiffness matrix are provided under the assumption of constant mass matrix. A numerical example is presented to validate the derived methods. In section “Conclusion,” the results of this study are summarized.

## Formulations and examples

### Estimation of updated stiffness and mass matrices

The dynamic equation for an undamped dynamic system of free vibration with  $n$  degrees of freedom (DOFs) can be expressed by

$$\mathbf{M}\ddot{\mathbf{q}} + \mathbf{K}\mathbf{q} = 0 \quad (1)$$

where  $\mathbf{M}$  and  $\mathbf{K}$  denote the  $n \times n$  mass and stiffness matrices, respectively;  $\ddot{\mathbf{q}}$  and  $\mathbf{q}$  are the  $n \times 1$  acceleration and displacement vectors, respectively. The equation describes the dynamic responses in the time domain.

The characteristic equation of the dynamic system may be written as

$$\mathbf{K}\boldsymbol{\phi} = \Lambda\mathbf{M}\boldsymbol{\phi} \quad (2)$$

where  $\boldsymbol{\phi}$  and  $\Lambda$  represent the  $n \times n$  mode shape matrices and  $\Lambda = \text{diag}(\omega_i^2)$  is the eigenmatrix and  $\omega_i$  ( $i = 1, 2, \dots, n$ ) is the  $i$ th modal frequency. The stiffness matrix  $\mathbf{K}$  and the flexibility matrix  $\mathbf{Q}$  may be expressed by Li et al.<sup>29</sup>

$$\mathbf{K} = \sum_{i=1}^n \mathbf{M}\omega_i^2 \boldsymbol{\phi}_i \boldsymbol{\phi}_i^T \mathbf{M} \quad (3)$$

$$\mathbf{Q} = \mathbf{K}^{-1} = \boldsymbol{\phi} \Lambda^{-1} \boldsymbol{\phi}^T = \sum_{i=1}^n \frac{\boldsymbol{\phi}_i \boldsymbol{\phi}_i^T}{\omega_i^2} \quad (4)$$

where the mode shape vectors are taken utilizing the mass normalization  $\boldsymbol{\phi}^T \mathbf{M} \boldsymbol{\phi} = \mathbf{I}$ , and  $\boldsymbol{\phi}_i$  is the  $i$ th mode shape vector. The modal contribution to the flexibility matrix in equation (4) decreases as frequency increases and the flexibility rapidly converges to a good approximation within the lowest few modes.

Taking the lowest  $l$  ( $l < n$ ) modes from the entire modes, the following equations from equations (2)–(4) can be derived by

$$\begin{bmatrix} \mathbf{K} & \mathbf{M} \end{bmatrix} \begin{bmatrix} \boldsymbol{\phi} \Lambda^{-1} \boldsymbol{\phi}^T & \boldsymbol{\phi} \\ 0 & -\boldsymbol{\phi} \Lambda \end{bmatrix} = \begin{bmatrix} \mathbf{I} & 0 \end{bmatrix} \quad (5)$$

where the matrix  $\mathbf{I}$  is an  $n \times n$  identity matrix,  $0$  is an  $n \times l$  zero matrix, and  $\Lambda$  is  $l \times l$  diagonal eigenmatrix.

The matrix  $\begin{bmatrix} \boldsymbol{\phi} \Lambda^{-1} \boldsymbol{\phi}^T & \boldsymbol{\phi} \\ 0 & -\boldsymbol{\phi} \Lambda \end{bmatrix}$  should be rank-deficient because the eigenmatrix of a few modes is taken. Thus, the updated parameter matrices  $\mathbf{M}$  and  $\mathbf{K}$  cannot be directly obtained by the inverse of equation (5).

The parameter matrices are derived by the least-squares method to minimize the performance index. In this study, the objective functions were utilized by combining the objective functions utilized by Berman and Nagy<sup>30</sup> and Caeser and Pete<sup>31</sup> as

$$D1 = \hat{\mathbf{M}}^{-1/2} (\hat{\mathbf{K}} - \mathbf{K}) \hat{\mathbf{M}}^{-1/2} \quad (6a)$$

$$D2 = \hat{\mathbf{M}}^{-1/2} (\hat{\mathbf{M}} - \mathbf{M}) \hat{\mathbf{M}}^{-1/2} \quad (6b)$$

$$D3 = \hat{\mathbf{K}}^{-1/2} (\hat{\mathbf{K}} - \mathbf{K}) \hat{\mathbf{K}}^{-1/2} \quad (6c)$$

$$D4 = \hat{\mathbf{K}}^{-1/2} (\hat{\mathbf{M}} - \mathbf{M}) \hat{\mathbf{K}}^{-1/2} \quad (6d)$$

where “ $\hat{\cdot}$ ” indicates the analytical parameter matrices. It is shown that the analytical mass and stiffness matrices are utilized as the weighting matrices.

This study compares the mathematical forms to describe the updated stiffness and mass matrices depending on the selected performance indices. Four different cases that combine the performance indices in equation (6) for predicting the stiffness and mass matrices are considered; (a) Case 1:  $D3 + D4$ , (b) Case 2:  $D3 + D2$ , (c) Case 3:  $D1 + D2$ , (d) Case 4:  $D1 + D4$ . The updated parameter matrices are independently derived according to the weighting matrices in the performance index. The performance index corresponding to Case 1 can be written by

$$D = \hat{\mathbf{K}}^{-1/2} (\hat{\mathbf{K}} - \mathbf{K}) \hat{\mathbf{K}}^{-1/2} + \hat{\mathbf{K}}^{-1/2} (\hat{\mathbf{M}} - \mathbf{M}) \hat{\mathbf{K}}^{-1/2} \quad (7)$$

To utilize the performance index of equation (7) into equation (5), equation (5) is modified as

$$\begin{bmatrix} \hat{\mathbf{K}}^{1/2} \hat{\mathbf{K}}^{-1/2} \mathbf{K} \hat{\mathbf{K}}^{-1/2} & \hat{\mathbf{K}}^{1/2} \hat{\mathbf{K}}^{-1/2} \mathbf{M} \hat{\mathbf{K}}^{-1/2} \end{bmatrix} \mathbf{R}_1 = \mathbf{P} \quad (8)$$

where  $\mathbf{R}_1 = \begin{bmatrix} \hat{\mathbf{K}}^{1/2} \boldsymbol{\phi} \Lambda^{-1} \boldsymbol{\phi}^T & \hat{\mathbf{K}}^{1/2} \boldsymbol{\phi} \\ 0 & -\hat{\mathbf{K}}^{1/2} \boldsymbol{\phi} \Lambda \end{bmatrix}$  and  $\mathbf{P} = [\mathbf{I} \ 0]$ .

Solving equation (8) with respect to  $[\hat{\mathbf{K}}^{1/2} \hat{\mathbf{K}}^{-1/2} \mathbf{K} \hat{\mathbf{K}}^{-1/2} \ \hat{\mathbf{K}}^{1/2} \hat{\mathbf{K}}^{-1/2} \mathbf{M} \hat{\mathbf{K}}^{-1/2}]$ , it can be derived by

$$\begin{bmatrix} \hat{\mathbf{K}}^{1/2} \hat{\mathbf{K}}^{-1/2} \mathbf{K} \hat{\mathbf{K}}^{-1/2} & \hat{\mathbf{K}}^{1/2} \hat{\mathbf{K}}^{-1/2} \mathbf{M} \hat{\mathbf{K}}^{-1/2} \end{bmatrix} = \mathbf{P} \mathbf{R}_1^+ + \mathbf{Y} (\mathbf{I} - \mathbf{R}_1 \mathbf{R}_1^+) \quad (9)$$

where “ $+$ ” denotes the Moore–Penrose inverse, and  $\mathbf{Y}$  is an  $n \times 2n$  arbitrary matrix.

Inserting the condition to minimize equation (7) into equation (9) and solving the result with respect to the arbitrary matrix, we obtain

$$\mathbf{Y} = \mathbf{P} \mathbf{R}_1^+ + \begin{bmatrix} \hat{\mathbf{K}}^{1/2} & \hat{\mathbf{M}} \hat{\mathbf{K}}^{-1/2} \end{bmatrix} (\mathbf{I} - \mathbf{R}_1 \mathbf{R}_1^+) + \mathbf{H} \mathbf{R}_1 \mathbf{R}_1^+ \quad (10)$$

where  $\mathbf{H}$  is another  $n \times 2n$  arbitrary matrix. Substituting equation (10) into equation (9) and arranging the result, it can be expressed by

$$\begin{bmatrix} \hat{\mathbf{K}}^{1/2} \hat{\mathbf{K}}^{-1/2} \mathbf{K} \hat{\mathbf{K}}^{-1/2} & \hat{\mathbf{K}}^{1/2} \hat{\mathbf{K}}^{-1/2} \hat{\mathbf{M}} \hat{\mathbf{K}}^{-1/2} \\ \mathbf{0} & \hat{\mathbf{K}}^{1/2} \end{bmatrix} (\mathbf{I} - \mathbf{R}_1 \mathbf{R}_1^+) = \mathbf{P} \mathbf{R}_1^+ + \begin{bmatrix} \hat{\mathbf{K}}^{1/2} & \hat{\mathbf{M}} \hat{\mathbf{K}}^{-1/2} \end{bmatrix} (\mathbf{I} - \mathbf{R}_1 \mathbf{R}_1^+) \quad (11)$$

Post-multiplying both sides of equation (11) by  $\begin{bmatrix} \hat{\mathbf{K}}^{1/2} & 0 \\ 0 & \hat{\mathbf{K}}^{1/2} \end{bmatrix}$ , the resulting stiffness and mass matrices can be derived by

$$\begin{bmatrix} \mathbf{K} & \mathbf{M} \end{bmatrix} = \left\{ \mathbf{P} \mathbf{R}_1^+ + \begin{bmatrix} \hat{\mathbf{K}}^{1/2} & \hat{\mathbf{M}} \hat{\mathbf{K}}^{-1/2} \end{bmatrix} (\mathbf{I} - \mathbf{R}_1 \mathbf{R}_1^+) \right\} \begin{bmatrix} \hat{\mathbf{K}}^{1/2} & 0 \\ 0 & \hat{\mathbf{K}}^{1/2} \end{bmatrix} \quad (12)$$

Equation (12) represents the mathematical forms of the parameter matrices that minimizes the performance index defined in equation (7). By the similar process as Case 1, the other cases can be similarly derived depending on the performance indices as

Case 2

$$D = \hat{\mathbf{K}}^{-1/2} (\hat{\mathbf{K}} - \mathbf{K}) \hat{\mathbf{K}}^{-1/2} + \hat{\mathbf{M}}^{-1/2} (\hat{\mathbf{M}} - \mathbf{M}) \hat{\mathbf{M}}^{-1/2} \quad (13a)$$

$$\begin{bmatrix} \mathbf{K} & \mathbf{M} \end{bmatrix} = \left\{ \mathbf{P} \mathbf{R}_2^+ + \begin{bmatrix} \hat{\mathbf{K}}^{1/2} & \hat{\mathbf{M}}^{1/2} \end{bmatrix} (\mathbf{I} - \mathbf{R}_2 \mathbf{R}_2^+) \right\} \begin{bmatrix} \hat{\mathbf{K}}^{1/2} & 0 \\ 0 & \hat{\mathbf{M}}^{1/2} \end{bmatrix} \quad (13b)$$

$$\mathbf{R}_2 = \begin{bmatrix} \hat{\mathbf{K}}^{1/2} \Phi \Lambda^{-1} \Phi^T & \hat{\mathbf{K}}^{1/2} \Phi \\ 0 & -\hat{\mathbf{M}}^{1/2} \Phi \Lambda \end{bmatrix}$$

Case 3

$$D = \hat{\mathbf{M}}^{-1/2} (\hat{\mathbf{K}} - \mathbf{K}) \hat{\mathbf{M}}^{-1/2} + \hat{\mathbf{M}}^{-1/2} (\hat{\mathbf{M}} - \mathbf{M}) \hat{\mathbf{M}}^{-1/2} \quad (14a)$$

$$\begin{bmatrix} \mathbf{K} & \mathbf{M} \end{bmatrix} = \left\{ \mathbf{P} \mathbf{R}_3^+ + \begin{bmatrix} \hat{\mathbf{K}} \hat{\mathbf{M}}^{-1/2} & \hat{\mathbf{M}}^{1/2} \end{bmatrix} (\mathbf{I} - \mathbf{R}_3 \mathbf{R}_3^+) \right\} \begin{bmatrix} \hat{\mathbf{M}}^{1/2} & 0 \\ 0 & \hat{\mathbf{M}}^{1/2} \end{bmatrix} \quad (14b)$$

$$\mathbf{R}_3 = \begin{bmatrix} \hat{\mathbf{M}}^{1/2} \Phi \Lambda^{-1} \Phi^T & \hat{\mathbf{M}}^{1/2} \Phi \\ 0 & -\hat{\mathbf{M}}^{1/2} \Phi \Lambda \end{bmatrix}$$

Case 4

$$D = \hat{\mathbf{M}}^{-1/2} (\hat{\mathbf{K}} - \mathbf{K}) \hat{\mathbf{M}}^{-1/2} + \hat{\mathbf{K}}^{-1/2} (\hat{\mathbf{M}} - \mathbf{M}) \hat{\mathbf{K}}^{-1/2} \quad (15a)$$

$$\begin{bmatrix} \mathbf{K} & \mathbf{M} \end{bmatrix} = \left\{ \mathbf{P} \mathbf{R}_4^+ + \begin{bmatrix} \hat{\mathbf{K}} \hat{\mathbf{M}}^{-1/2} & \hat{\mathbf{M}} \hat{\mathbf{K}}^{-1/2} \end{bmatrix} (\mathbf{I} - \mathbf{R}_4 \mathbf{R}_4^+) \right\} \begin{bmatrix} \hat{\mathbf{M}}^{1/2} & 0 \\ 0 & \hat{\mathbf{K}}^{1/2} \end{bmatrix} \quad (15b)$$

$$\mathbf{R}_4 = \begin{bmatrix} \hat{\mathbf{M}}^{1/2} \Phi \Lambda^{-1} \Phi^T & \hat{\mathbf{M}}^{1/2} \Phi \\ 0 & -\hat{\mathbf{K}}^{1/2} \Phi \Lambda \end{bmatrix}$$

Equations (12)–(15) represent the established performance indices and the corresponding mathematical forms to describe the updated parameter matrices. The parameter matrices take different forms depending on the weighting matrices. The numerical comparison is performed in the example.

**Example 1.** The correction methods of the parameter matrices proposed in this study are compared depending on the objective functions in the finite-element model of a fixed-end beam, as shown in Figure 1, whose applicability in the detection of damaged elements is examined. The beam length is 1 m, the length of each beam element is 20 mm, and the beam is modeled by 50 beam elements. The nodal points and elements are numbered in the figure. Each node has two DOFs of vertical displacement and slope, but the slope is neglected because it exhibits difficulty in collecting the rotational responses in the actual structure. The beam has an elastic modulus of  $2.1 \times 10^5$  MPa, its gross cross-section is  $b \times h = 50 \text{ mm} \times 12 \text{ mm}$ , and its

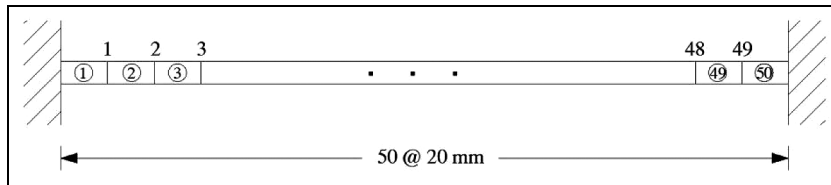


**Figure 1.** A fixed-end beam structure model.

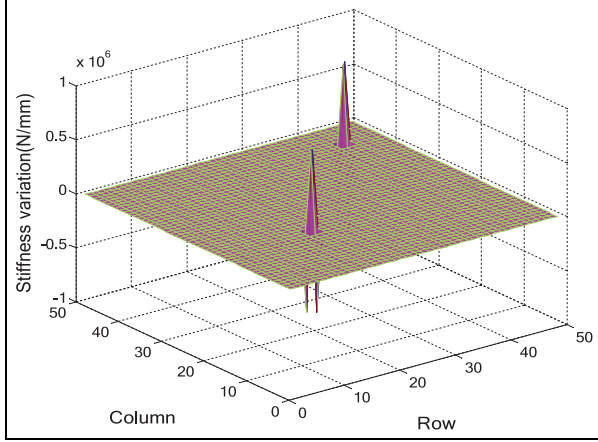


**Figure 2.** Variation between actual and analytical stiffness matrices.

damage section is established as  $b \times h = 50 \text{ mm} \times 10.5 \text{ mm}$ . This example compares the numerical results of the four cases of equations (12)–(15), depending on the number of measurement data by only the first entire modal data and the lowest two entire modal data sets. We assume multiple damages of 20% section loss at elements ⑬ and ④③.

The difference between the analytical and actual stiffness matrices at the damaged state is plotted in Figure 2. It is observed that, where the abrupt change in the parameter matrices is located at the damaged elements.

The parameter matrices are updated using the noise-free first modal data only as the measurement data. The plots in Figure 3 represent the differences between the analytical and estimated parameter matrices. The proposed methods do not accurately describe the parameter matrices. The plots in Figure 3 compare the parameter matrices of the four cases estimated using the noise-free first modal data only. The variations in the stiffness and mass matrices exhibit different values depending on the weighting matrices. It is observed that the difference in the parameter matrices is decreased in using the analytical stiffness matrix as the weighting matrix rather than the analytical mass matrix, as shown in the updated stiffness and mass matrix plots in Case 1 (Cases 1-K and 1-M), updated stiffness matrix plot in Case 2 (Case 2-K), and updated stiffness matrix plot in Case 2 (Case 2-K). The damaged elements are located at the elements to exhibit the abrupt change in the parameter matrices. The updated stiffness and mass matrices exhibit significant differences when the analytical mass matrix is used as the weighting matrix, so the variation plots rarely provide the damage information, as listed in Figure 3.

Figure 4 lists the differences between the parameter matrices predicted using the lowest two modal data sets as the measurement data; noise-free measurement data are assumed. The plots considering the analytical stiffness matrix as the weighting matrix show that the parameter matrices yield more accurate results with an increase in the number of mode shapes that participate in updating them. It is expected that the estimation of the updated parameter matrices gradually approaches the actual ones with an increase in the measured mode number.

Table 1 lists the suitability of the weighting matrix to update the parameter matrices synthesizing the results listed in Figures 3 and 4, where “○/A” and “X/B” indicate the suitability and unsuitability of matrices A and B as the weighting matrices, respectively. It is observed that the utilization of the stiffness matrix provides more reasonable results.

This study also investigates the effect of external noise contained in the measured mode shapes. The errors included in the measured data lead to some deviations from the analytical results. A simulated data set is established by adding a series of random numbers to represent errors in the calculated mode shape data. The  $i$ th measured mode shape vector  $\boldsymbol{\varphi}_i^m$  can be calculated from the analytical mode shape vector  $\boldsymbol{\varphi}_i^0$  as

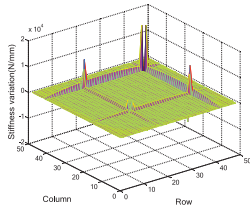
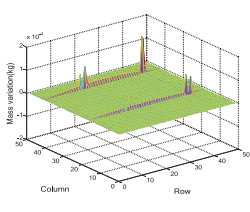
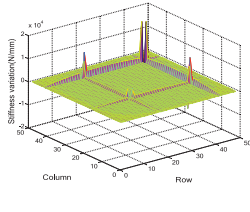
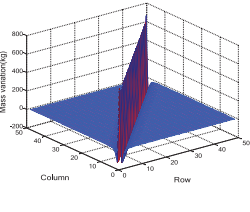
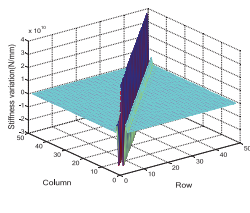
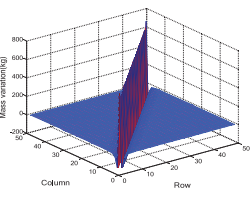
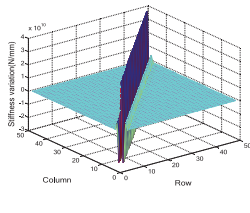
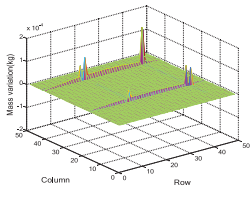
$$\boldsymbol{\varphi}_i^m = \boldsymbol{\varphi}_i^0(1 + \alpha\sigma) \quad (16)$$

where  $\alpha$  denotes the relative magnitude of the error and  $\sigma$  is a random number variant in the range  $[-1, 1]$ .

Figure 5 lists the variations in the stiffness and mass matrices estimated using the lowest two modal data sets contaminated by 2% noise level in equation (16), where “Case $\alpha - \beta$ ” indicates the case number ( $\alpha = 1, 2, 4$ ) and the updated parameter matrices ( $\Delta = \mathbf{K}$  and  $\mathbf{M}$ ). The analytical stiffness matrix is utilized as the weighting matrix from the results listed in Table 1. The irregular variations in the parameter matrices indicate the existence of the external noise. This example detects the damage based on the stiffness and mass variations mixed with the noise.

Figure 5 shows the variation matrix between the analytical and updated parameter matrices estimated using the lowest two modal data sets of 2% noise level. It displays the stiffness and mass curves corresponding to the diagonal elements in the parameter matrices and their curvature in Figure 5, respectively, using a central difference approximation

$$C_{i+1} = \frac{\Delta a_i - 2(\Delta a_{i+1}) + \Delta a_{i+2}}{h^2}, i = 1, 2, \dots, 47, \\ \Delta a_i = \mathbf{M}(i, i) - \hat{\mathbf{M}}(i, i) \text{ or } \mathbf{K}(i, i) - \hat{\mathbf{K}}(i, i) \quad (17)$$

	$\Delta K$	$\Delta M$
Case 1		
	Weighting matrix: $\hat{K}$	Weighting matrix: $\hat{K}$
Case 2		
	Weighting matrix: $\hat{K}$	Weighting matrix: $\hat{M}$
Case 3		
	Weighting matrix: $\hat{M}$	Weighting matrix: $\hat{M}$
Case 4		
	Weighting matrix: $\hat{M}$	Weighting matrix: $\hat{K}$

**Figure 3.** Variations in parameter matrices estimated using noise-free first modal data only. The labels in the x and y axes indicate the row and column in the stiffness and mass matrices, respectively.

where  $C_i$  is the second derivative of the  $i$ th flexural dimension corresponding to the diagonal elements in the parameter variation matrices, and  $h$  is the distance between two successive nodes.

The effect of 2% noise level is investigated considering the cases listed in Table 1. The variation curves in the stiffness and mass matrices exhibit an abrupt change at the damaged elements in Figure 6(a), (c),

(e), and (g). Similarly, the curvature curves in Figure 6(b), (d), (f), and (h) provide information on the damaged elements. A comparison of the variation curves indicates that the utilization of the updated stiffness matrix in Figure 5(a) and (e) provides more accurate damage information than the updated mass matrix in Figure 6(c) and (g) despite the external noise.

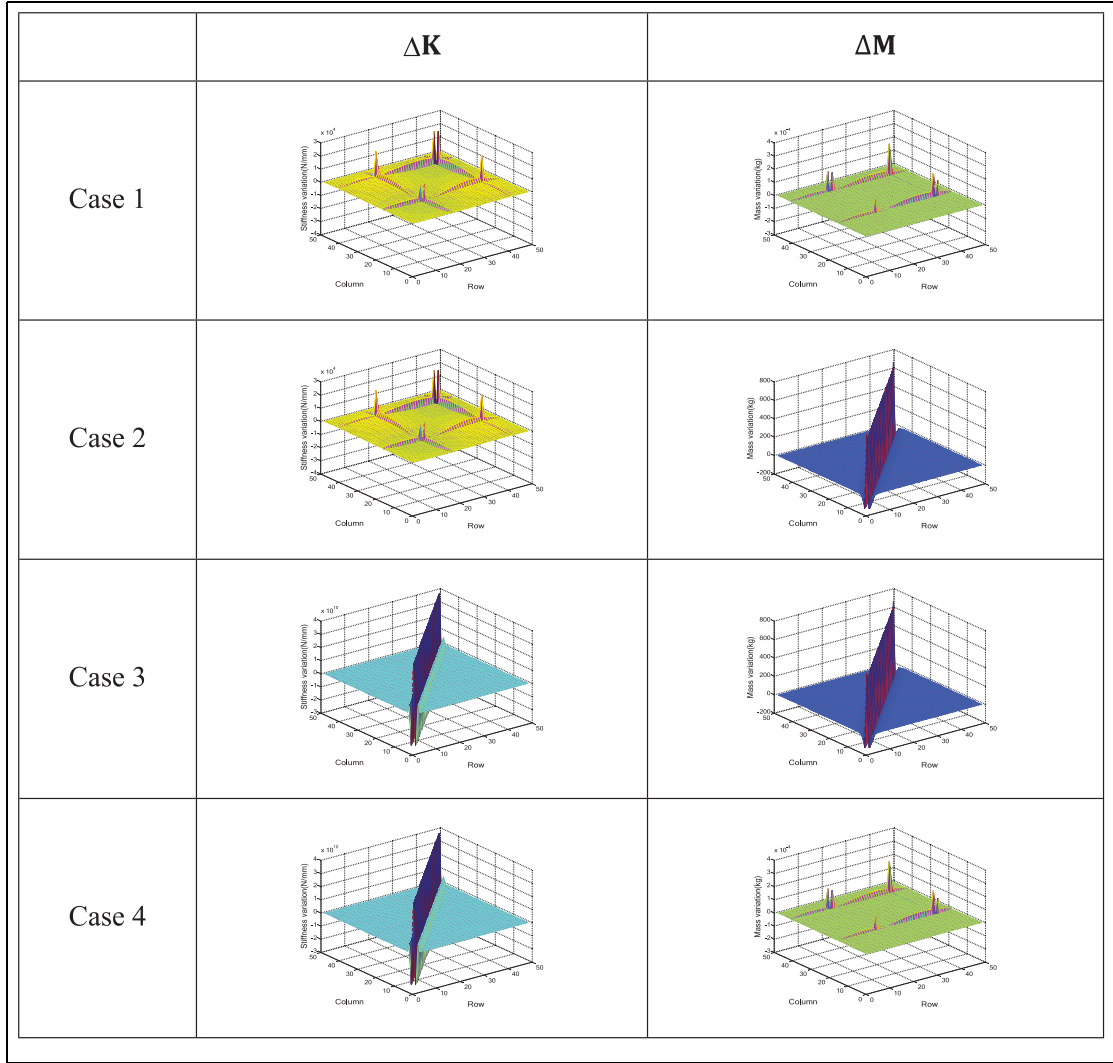


**Figure 4.** Variations in parameter matrices estimated using two noise-free measured modal data. The labels in the x and y axes indicate the row and column in the stiffness and mass matrices, respectively.

**Table 1.** Comparison of the suitability of weighting matrices.

Estimated parameter matrices	Case 1	Case 2	Case 3	Case 4
M	○	×	×	○
K	○	○	×	×

“○/A” and “X/B” indicate the suitability and unsuitability of the matrices A and B as the weighting matrices, respectively.

### Estimation of updated stiffness matrix

Assuming the invariant mass  $\mathbf{M} = \hat{\mathbf{M}}$  and lowest  $m(m < n)$  modal data sets as the measurement data, equation (4) can be approximately written in the matrix form as

$$\mathbf{K}\mathbf{Q} = \mathbf{I} \quad (18)$$

where  $\mathbf{A} = \sum_{i=1}^m \omega_i^2$ ,  $\mathbf{Q} = \sum_{i=1}^m (1/\omega_i^2) \Phi_i \Phi_i^T$ , and  $\mathbf{I}$  is the  $n \times n$  identity matrix. Equation (18) can be regarded as the constraint condition to describe the dynamic characteristics of the system. The matrix  $\mathbf{Q}$  in equation (18) should be rank deficient.

The updated stiffness matrix  $\mathbf{K}$  in equation (18) is derived by minimizing the performance index as



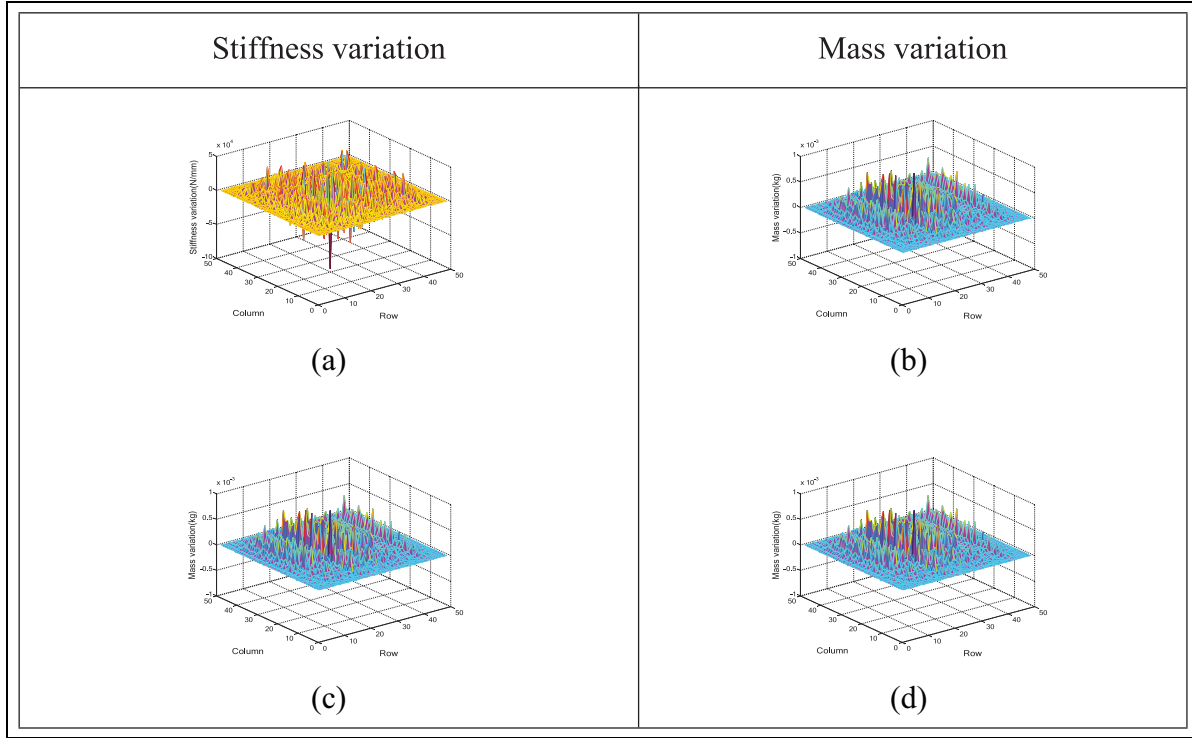


**Figure 5.** Variations in parameter matrices estimated using the lowest two modal data contaminated by 2% noise: (a) Case I-K, (b) Case I-M, (c) Case 2-K, and (d) Case 4-M.

The labels in the x and y axes indicate the row and column in the stiffness and mass matrices, respectively.

$$\mathbf{P} = \hat{\mathbf{K}}^{-1/2} (\hat{\mathbf{K}} - \mathbf{K}) \hat{\mathbf{K}}^{-1/2} \quad (19)$$

As indicated in the previous example, the analytical stiffness matrix  $\hat{\mathbf{K}}$  is utilized as the weighting matrix.

The constraint equation (18) is not related to the specific mode independently but is established by the modal data accumulated in the specific  $m$ th mode. Thus, the constraint interdependently affects the modal data within the  $m$ th mode. The stiffness variation matrix is derived by inserting the constraint condition of equation (18) into the performance index.

To insert the condition to minimize the performance index of equation (19), equation (18) is modified as

$$\hat{\mathbf{K}}^{1/2} \hat{\mathbf{K}}^{-1/2} \mathbf{K} \hat{\mathbf{K}}^{-1/2} \mathbf{R} = \mathbf{I} \quad (20)$$

where  $\mathbf{R} = \hat{\mathbf{K}}^{1/2} \mathbf{Q}$ .

Solving equation (20) with respect to  $\hat{\mathbf{K}}^{1/2} \hat{\mathbf{K}}^{-1/2} \mathbf{K} \hat{\mathbf{K}}^{-1/2}$  using the generalized inverse solution yields

$$\hat{\mathbf{K}}^{1/2} \hat{\mathbf{K}}^{-1/2} \mathbf{K} \hat{\mathbf{K}}^{-1/2} = \mathbf{R}^+ + \mathbf{y} [\mathbf{I} - \mathbf{R} \mathbf{R}^+] \quad (21)$$

where  $\mathbf{y}$  is the  $n \times n$  arbitrary matrix, and  $\mathbf{I}$  represents the  $n \times n$  identity matrix. Equation (21) indicates an infinite number of solutions on the stiffness variation. This study derives the mathematical form of the

updated stiffness matrix to minimize the performance index of equation (19).

Applying the minimization condition of equation (19) into equation (21), the arbitrary matrix  $\mathbf{y}$  yields

$$\mathbf{y} = [\hat{\mathbf{K}}^{1/2} - \mathbf{R}^+] [\mathbf{I} - \mathbf{R} \mathbf{R}^+] + \mathbf{h} \mathbf{R} \mathbf{R}^+ \quad (22)$$

where  $\mathbf{h}$  is the  $n \times n$  arbitrary matrix and  $\mathbf{R}^+ \mathbf{R} \mathbf{R}^+ = \mathbf{R}^+$ . Substituting equation (22) into equation (21) and arranging the result, we get

$$\hat{\mathbf{K}}^{1/2} \hat{\mathbf{K}}^{-1/2} \mathbf{K} \hat{\mathbf{K}}^{-1/2} = \hat{\mathbf{K}}^{1/2} + [\mathbf{I} - \hat{\mathbf{K}}^{1/2} \mathbf{R}] \mathbf{R}^+ \quad (23)$$

Post-multiplying both sides of equation (23) by  $\hat{\mathbf{K}}^{1/2}$  and arranging the result, we obtain

$$\mathbf{K} = \hat{\mathbf{K}} + [\mathbf{I} - \hat{\mathbf{K}} \mathbf{Q}] (\hat{\mathbf{K}}^{1/2} \mathbf{Q})^+ \hat{\mathbf{K}}^{1/2} \quad (24)$$

The second term on the right-hand side of equation (24) represents the variation in the stiffness matrix owing to the deterioration of structural performance, external noise, construction, and measurement errors. The modal data are related to the stiffness variation. The variable  $\mathbf{Q}$  of equation (24) indicates that the updated stiffness matrix is sensitive to the number of selected modes.



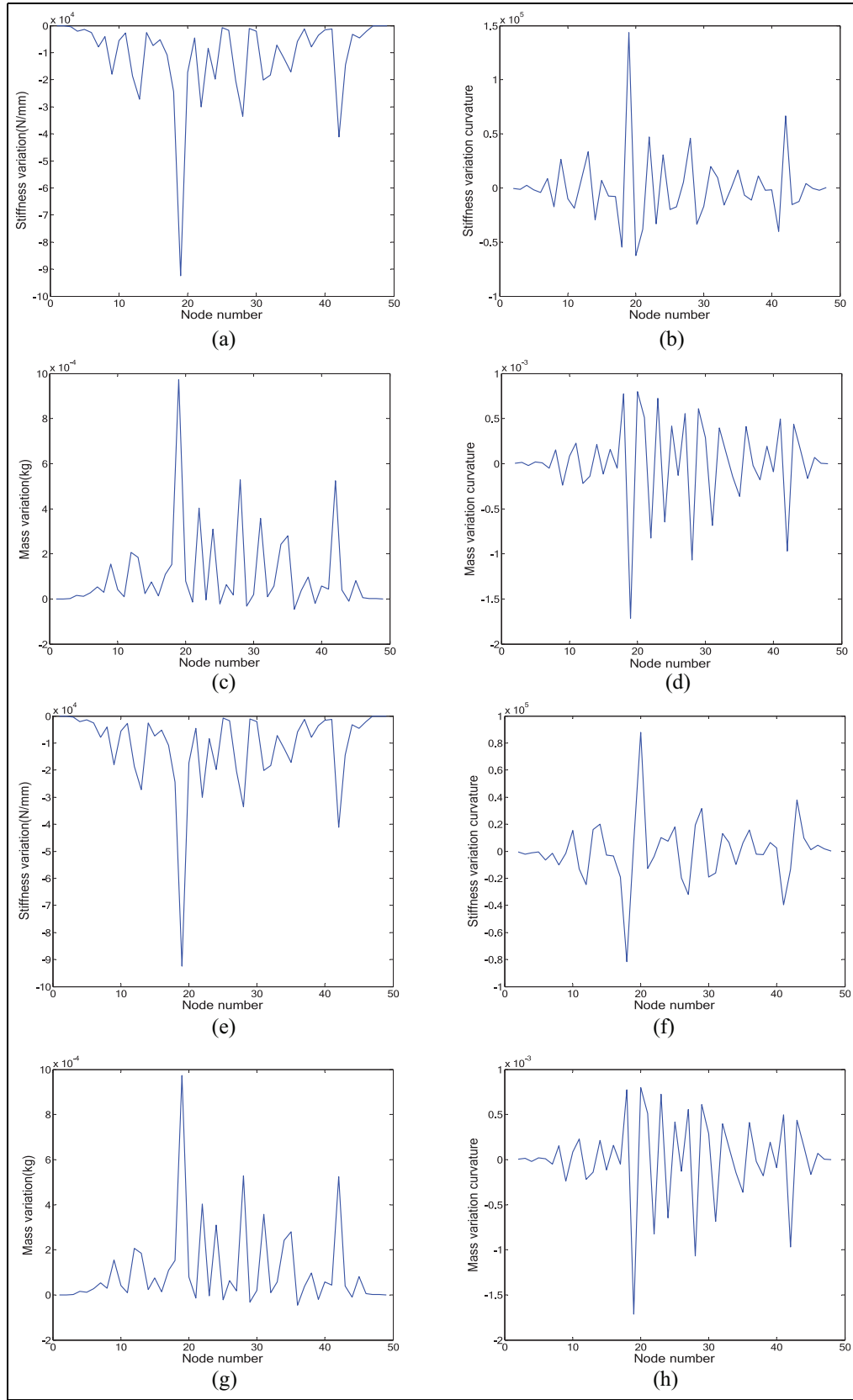


**Figure 6.** Diagonal elements in variation matrices between analytical and estimated parameters using 2% noise level and the first two modal data sets: (a) Case I-K, (b) curvature of Case I-K, (c) Case I-M, (d) curvature of Case I-M, (e) Case 2-K, (f) curvature of Case 2-K, (g) Case 4-M, and (h) curvature of Case 4-M.

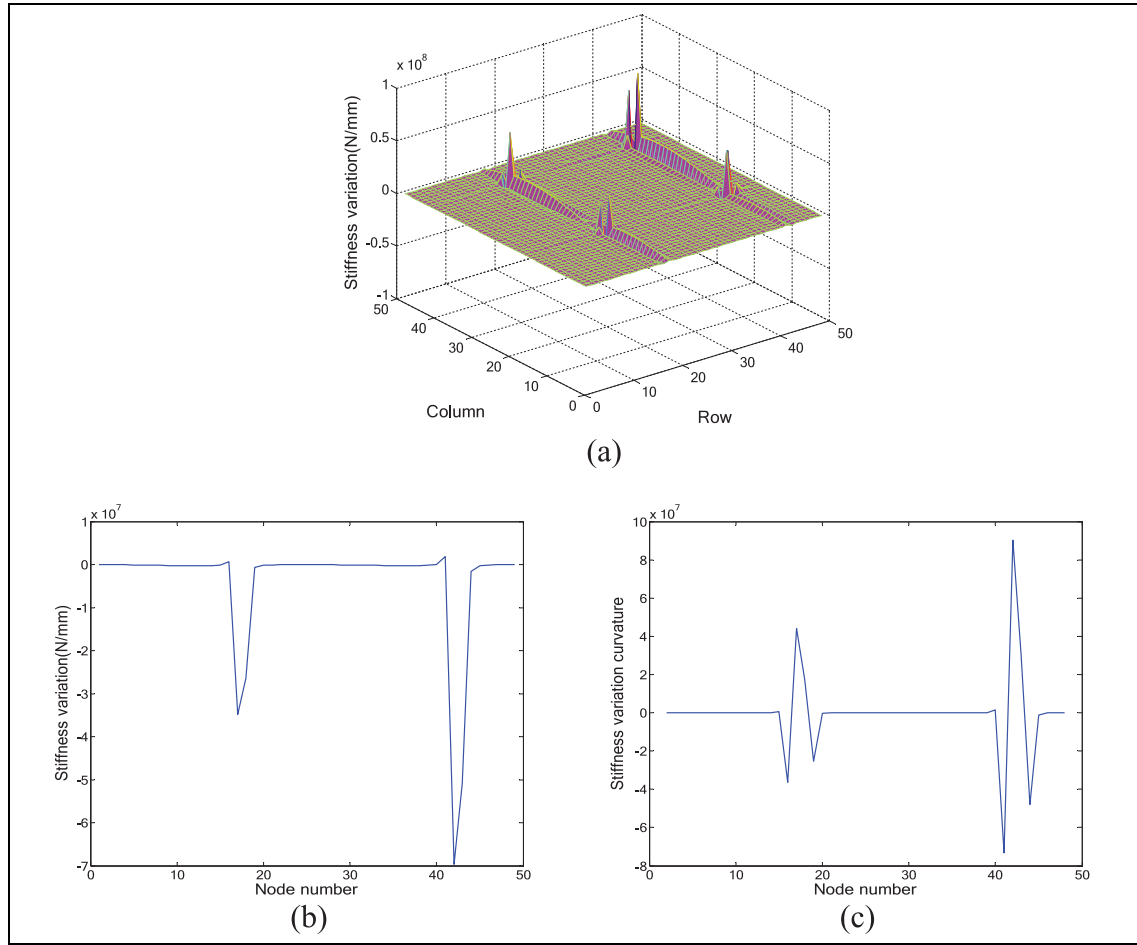


**Figure 7.** Numerical results using noise-free measurement data: (a) stiffness variation matrix, (b) diagonal elements in the stiffness variation matrix and (c) curvature of diagonal elements.

**Example 2.** The second example considers damage detection using the stiffness variation alone. Assuming the invariant mass matrix, this example evaluates the numerical results of the updated methods by the lowest two modal data sets depending on the external noise. The measured modal data replaced by the numerically simulated data are utilized to estimate the stiffness matrix. The numerical experiments update the stiffness matrix using the lowest two modes (F-2 beam model). The responses of the F-2 beam model are constrained by the lowest two natural frequencies and the corresponding mode shapes.

The stiffness matrix of the F-2 beam model is updated by equation (24) and noise-free measurement modal data. Figure 7(a) shows the stiffness variation matrix before and after the damage occurrence. This shows that the abrupt change in the stiffness is limited to the damaged elements. The proposed approach does not yield accurate stiffness variations compared to the actual variations because the beam model is constrained by the lowest two modal data sets only. The

abrupt variations are found at the damaged elements by the curve of the diagonal elements in the stiffness variation matrix and its curvature curve, as shown in Figure 7(b) and (c), respectively. As shown in the plots, the damage can be accurately detected by the stiffness variations in the case of noise-free measurement data.

The external noise contained in the measured mode shape data leads to the deviation in the actual stiffness as well as the actual modal data. Figure 8(a) shows the estimated stiffness variations including 2.0% noise, where the irregularity in the stiffness variations is observed unlike the noise-free case. The plots display the sensitivity to external noise. Figure 8(b) and (c) shows the numerical results using the lowest two modal data only contaminated by 2% noise level. It is expected that the damages are located in the neighborhood of element 28, except for the actual damaged elements 18 and 43, as shown in Figure 8(b) and (c). This is caused by the external noise, and the inaccuracy of damage detection disappears in the use of accumulated data through repeated numerical simulations. It is

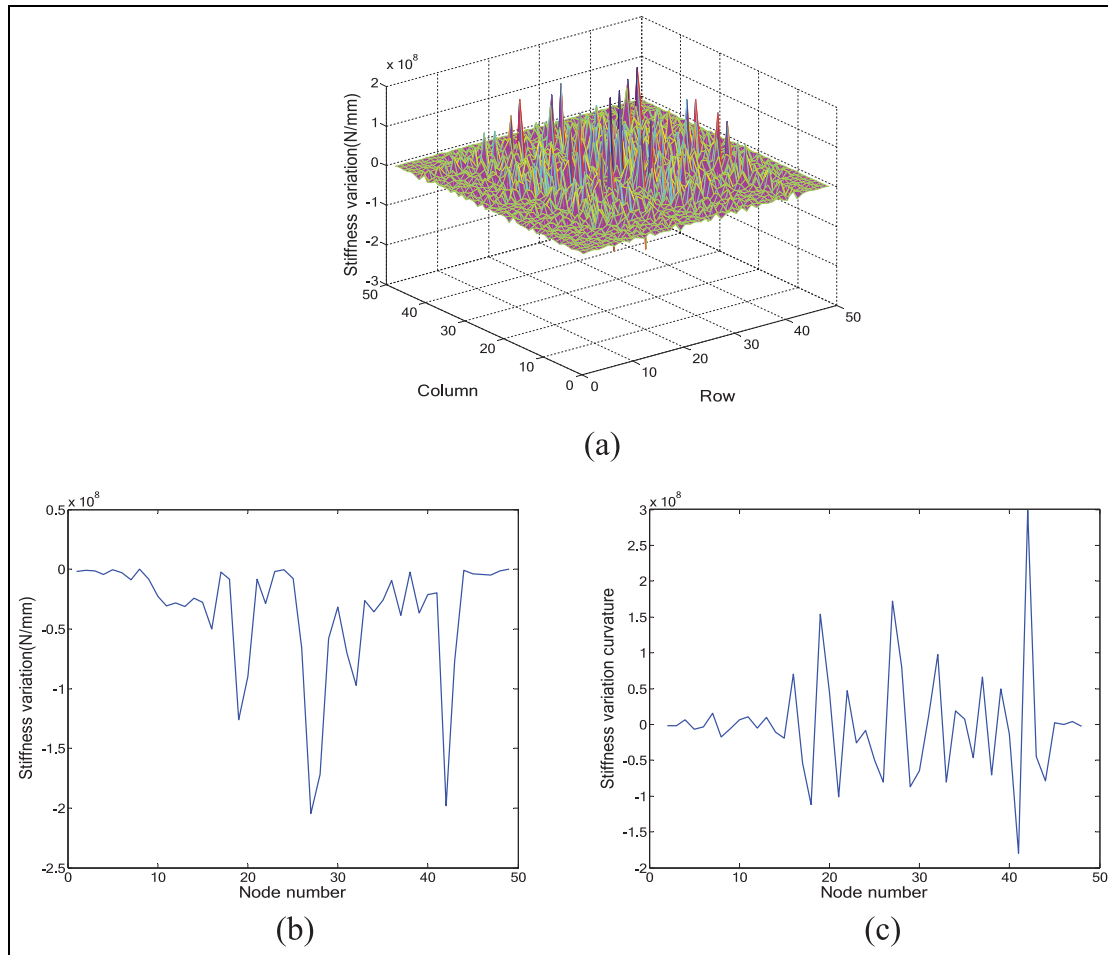


**Figure 8.** Numerical results using 2% noise-contaminated measurement data: (a) stiffness variation matrix, (b) diagonal elements in the stiffness variation matrix, and (c) curvature of diagonal elements.

found that the proposed method for updating the stiffness matrix can be utilized in detecting the damage despite the external noise.

## Conclusion

The dynamic responses of the analytical model do not coincide with the actual ones, and the dynamic parameter matrices should be corrected for subsequent analyses. This article proposes the mathematical forms for updating the stiffness and mass matrices. However, the method rarely provides accurate parameter matrices. It is shown that the parameter matrices are straightforwardly derived and take explicitly different forms depending on the weighting matrices in the objective functions. In comparing the variation curves to utilize the stiffness and mass matrices, it is observed that the stiffness matrix as the weighting matrix indicates more accurate damage information than the mass matrix despite the external noise. In addition, the method in section “Estimation of updated stiffness matrix” to

update the stiffness matrix can only also be utilized in detecting the damage despite the external noise. It is not practical to collect the data of a full set of DOFs. More research on the update of parameter matrices is required because of using fewer measurement data than the system DOF.

## Declaration of conflicting interests

The author(s) declared no potential conflicts of interest with respect to the research, authorship, and/or publication of this article.

## Funding

The author(s) disclosed receipt of the following financial support for the research, authorship, and/or publication of this article: This research is supported by the Basic Science Research Program through the National Research Foundation of Korea (NRF) funded by the Ministry of Education (grant no. NRF-2016R1D1A1A09918011) and also by the 2018 Research Grant (PoINT) from Kangwon National University.

## ORCID iD

Hee-Chang Eun  <https://orcid.org/0000-0003-0701-9233>

## References

- Wang XJ, Zhou XQ, Xia Y, et al. Comparisons between modal-parameter-based and flexibility-based damage identification methods. *Adv Struct Eng* 2016; 16: 1611–1619.
- Schommer S, Mahowald J, Nguyen VH, et al. Health monitoring based on dynamic flexibility matrix: theoretical models versus in-situ tests. *Engineering* 2017; 9: 37–67.
- Lekidis V, Karakostas C, Christodoulou K, et al. Investigation of dynamic response and model updating of instrumented R/C bridges. In: *Proceedings of the 13th world conference on earthquake engineering*, 1–6 August 2004, Vancouver, BC, Canada. Vancouver, BC, Canada: WCEE.
- Başağa HB, Türker T and Bayraktar A. A model updating approach based on design points for unknown structural parameters. *Appl Math Model* 2011; 35: 5872–5883.
- Fuentes HP. Application of the mode-shape expansion based on model order reduction methods to a composite structure. *Open Eng* 2017; 7: 199–212.
- Rim SK, Eun HC and Lee ET. Estimation of mode shapes expanded from incomplete measurements. *J Vibroeng* 2014; 16: 2123–2129.
- Chen HP and Tee KF. Structural finite element model updating using incomplete ambient vibration modal data. *Sci China Technol Sc* 2014; 57: 1677–1688.
- Sheinman I. Damage detection and updating of stiffness and mass matrices using mode data. *Comput Struct* 1996; 59: 149–156.
- Pokharkar PV and Shrikhande M. Structural health monitoring via stiffness update. *ISSET J Earthq Technol* 2010; 47: 47–60.
- Sung SH, Koo KY and Jung HJ. Modal flexibility-based damage detection of cantilever beam-type structures using baseline modification. *J Sound Vib* 2014; 333: 4123–4138.
- Rainieri C, Fabbrocino G and Verderame GM. Non-destructive characterization and dynamic identification of a modern heritage building for serviceability seismic analyses. *NDT E Int* 2013; 60: 17–31.
- Katebi L, Tehranizadeh M and Mohammadgholibeyki N. A generalized flexibility matrix-based model updating method for damage detection of plane truss and frame structures. *J Civ Struct Health Monit* 2018; 8: 301–314.
- Chen B and Nagarajaiah S. Flexibility-based structural damage identification using Gauss-Newton method. *Sadhana* 2013; 38: 557–569.
- Li J, Li Z, Zhong H, et al. Structural damage detection using generalized flexibility matrix and changes in natural frequencies. *AIAA J* 2012; 50: 1072–1078.
- Yang QW and Sun BX. Structural damage identification based on best achievable flexibility change. *Appl Math Model* 2011; 35: 5217–5224.
- Cao Z, Fei Q, Jiang D, et al. Substructure-based model updating using residual flexibility mixed-boundary method. *J Mech Sci Technol* 2017; 31: 759–769.
- Yang CS, Zhou L and Wang GS. A flexibility-based method for damage identification of cantilever-type structures. *J Netw* 2014; 9: 3120–3126.
- Lacidogna G, Piana G and Carpinteri A. Damage monitoring of three-point bending concrete specimens by acoustic emission and resonant frequency analysis. *Eng Fract Mech* 2019; 210: 203–211.
- Lacidogna G, Piana G and Carpinteri A. Acoustic emission and modal frequency variation in concrete specimens under four-point bending. *Appl Sci* 2017; 7: 339.
- Rainieri C and Fabbrocino G. Automated output-only dynamic identification of civil engineering structures. *Mech Syst Signal Process* 2010; 24: 678–695.
- Rainieri C and Fabbrocino G. Development and validation of an automated operational modal analysis algorithm for vibration-based monitoring and tensile load estimation. *Mech Syst Signal Process* 2015; 60–61: 512–534.
- Rainieri C, Magalhaes F, Gargaro D, et al. Predicting the validity of natural frequencies and its causes by second-order blind identification. *Struct Health Monit* 2019; 18: 486–507.
- Mohammad F, Moradi L, Baleanu D, et al. A hybrid functions numerical scheme for fractional optimal control problems: application to nonanalytic dynamic systems. *J Sound Vib* 2017; 24: 5030–5043.
- Baleanu D and Shiri B. Collocation methods for fractional differential equations involving non-singular kernel. *Chaos Soliton Fract* 2018; 116: 136–145.
- Baleanu D, Shiri B, Srivastava HM, et al. A Chebyshev spectral method based on operational matrix for fractional differential equations involving non-singular Mittag-Leffler kernel. *Adv Differential Equ* 2018; 2018: 353.
- Baleanu D, Caponetto R and Machado JAT. Challenges in fractional dynamics and control theory. *J Vib Control* 2016; 22: 2151–2152.
- Baleanu D, Ahmad B, Nieto JJ, et al. Advanced topics in dynamics of complex systems. *Math Probl Eng* 2014; 2014: 354712.
- Jajarmi A, Hajipour M, Sajjadi SS, et al. A robust and accurate disturbance damping control design for non-linear dynamical systems. *Optim Contr Appl Met* 2019; 40: 375–393.
- Li J, Li Z, Zhong H, et al. Structural damage detection using generalized flexibility matrix and changes in natural frequencies. *AIAA J* 2012; 50: 1072–1078.
- Berman J and Nagy EJ. Improvement of a large analytical model using test data. *AIAA J* 1983; 21: 1168–1173.
- Caeser B and Pete J. Direct update of dynamic mathematical models from modal test data. *AIAA J* 1987; 25: 1494–1499.